Accepted Manuscript

International Journal of Structural Stability and Dynamics

Article Title:	Automated health condition diagnosis of in-situ wood utility poles using an intelligent non-destructive evaluation (NDE) framework
Author(s):	Yang Yu, Mahbube Subhani, Azadeh Noori Hoshyar, Jianchun Li, Huan Li
DOI:	10.1142/S021945542042002X
Received:	04 October 2019
Accepted:	25 March 2020
To be cited as:	Yang Yu *et al.*, Automated health condition diagnosis of in-situ wood utility poles using an intelligent non-destructive evaluation (NDE) framework, *International Journal of Structural Stability and Dynamics*, doi: 10.1142/S021945542042002X
Link to final version:	https://doi.org/10.1142/S021945542042002X

World Scientific
www.worldscientific.com

Automated health condition diagnosis of in-situ wood utility poles using an intelligent non-destructive evaluation (NDE) framework

Yang Yu[1], Mahbube Subhani[2], Azadeh Noori Hoshyar[3], Jianchun Li[1,*], Huan Li[1]

[1]Centre for Built Infrastructure Research, Faculty of Engineering and IT, University of Technology Sydney, Ultimo, NSW 2007, Australia
[2]School of Engineering, Deakin University, Geelong, VIC 3125, Australia
[3]School of Science, Engineering & Information Technology, Federation University Australia, BrisbaneCity, QLD 4001, Australia
[*]Corresponding author: jianchun.li@uts.edu.au

Abstract

Wood utility poles are widely applied in power transmission and telecommunication systems in Australia. Because of a variety of external influence factors, such as fungi, termite and environmental conditions, failure of poles due to the wood degradation with time is of common occurrence with high degree uncertainty. The pole failure may result in serious consequences including both economic and public safety. Therefore, accurately and timely identifying the health condition of the utility polesis of great significance for economic and safe operation of electricity and communication networks. In this paper, a novel non-destructive evaluation (NDE) frameworkwith advanced signal processing and artificial intelligence (AI) techniques is developed to diagnose the condition of utility pole in field.To begin with, the guided waves (GWs) generated within the pole is measured using multi-sensing technique, avoiding difficult interpretation of various wave modes which cannot be detected by only one sensor. Then, empirical mode decomposition (EMD) and principal component analysis (PCA) are employed to extract and select damage-sensitive features from the captured GW signals. Additionally, the up-to-date machine learning (ML) techniques are adopted to diagnose the health condition of the pole based on selected signal patterns. Eventually, the performance of the developed NDE framework is evaluated using the field testing data from 15 new and 24 decommissioned utility poles at the pole yard in Sydney.

Keywords: Wood electricity pole; non-destructive evaluation; guided wave; advanced signal processing; machine learning

1. Introduction

Woodutility poles are essential infrastructure for power distribution and telecommunication networks. There are over 5 million wood poles in Australia, representing 80% of the total poles in use.[1,2] Around 70% of these wood poles were installed before 1965 and will need replacement or maintenance in the near future. As the associated costs may reach up to $1.75 billion,[3,4] it is economically advantageous to extend the in-service life of wood poles as long as possible. Current methods of testing do not provide the consistent accuracy required to ensure public safety and may result in the decommissioning of serviceable poles.

The challenges in developing a reliable solution for non-destructive evaluation (NDE) of wood poles include, but are not limited to, anisotropic properties of wood as a material, variation in species used for power poles, differences in the properties of surrounding soil, varying length and diameter of poles across the distribution network and the hardware attached to the poles (e.g. conductors and cross-arms). Further, environmental factors, including moisture and temperature,can lead to variation of material properties even for the same timber species and geometrical conditions.[5,6]Lastly, different types of damage contribute to different signatures of structural properties. Accordingly, when the damage-sensitive features are affected by the aforementioned factors, it becomes extremely complex for damage identification in the structure.[7,8]

Guided wave (GW)-based techniques have been widely used for pile-type structures,[9] which may also be a feasible solution to internal damage detection at unreachable locations of round poles based on GW propagation. In this technique, the structure is struck manually by a modal hammer which induces broadband and low frequency (long wavelength) input.[10,11] When the wavelength of the input signal is more than the diameter of the structure, the induced stress wave causes a standing wave within the pole that leads to vibration of the whole structure.[12] Accordingly, the broadband GW signal has sufficient energy to ensure that the induced energy can travel through the whole structure and therefore, when a sensor is placed locally it will capture information of the whole structure. Generally, the GW-based methods can be categorized as longitudinal wave (LW) and

bending wave (BW).[13–16] The LW is generated by the vertical force induced from the top of the structure, which is reflected and captured by the sensor installed near the impact location. The BW (also called flexural wave) is generated by the traversal force, which is collected by the sensor installed at the side of the structure. The BW is often employed for the case where the top of the structure is out of reach. Nevertheless, it is of high dispersion in essence and needs signal processing techniques to analyze complicated wave behaviours.

In reality, the wood utility polesare generally 12–15 m long with 1.5–2 m embedded in the soil. Consequently, it is not realistic to induce the impact force from the top of the pole by the impact hammer to generate the LW. Alternatively, the hammer strike is exposed to the side surface of pole at a height that can be reached, which can generate the BW with complicated wave behaviours including two-directional wave propagation meanwhile,multiple modes with broad frequency bands and dispersion characteristics. Hence, it is challenging to process such type of complicated waves using physical-based approaches for the pole condition diagnosis. In this study, alternatively, the data driven-based approaches are investigated to fix this issue for the task of interest. First of all, the empirical mode decomposition (EMD) method is utilized to decompose the transverse GWs captured from multiple sensors into several intrinsic mode functions (IMFs) and a residue. For the first three IMFs, the signal energy ratio is calculated as the signal patterns that can be correlated with pole health condition. To resolve the problem of mode mixing problem and avoid the pseudo IMFs extracted from raw wave signals, a modified EMD is proposed by evaluating the correlation between raw signal and IMFs to eliminate the pseudo ones. Then, principal component analysis (PCA) technique is employed to decrease the redundant information from different sensors and select optimal features as the inputs of diagnosis models.The state-of-the-art machine learning approaches are also used to develop predictive models for health diagnosis of wood poles in the field. Finally, 15 new poles and 24 decommissioned poles are tested and autopsied in a pole yard in Sydney, and the collected data are adopted to assess the capacity of developed framework.

2. Guide wave propagation in cylinder wood structures

Traditional GW-based NDE techniques are mainly on basis of the theory of 1-dimentional (1D) wave propagation, which was developed according to the deformation kinematics.[17] In this theory, the wave is supposed to propagate like the plane in one direction with similar amplitude in other directions, the schematic of which is presented in Fig. 1.

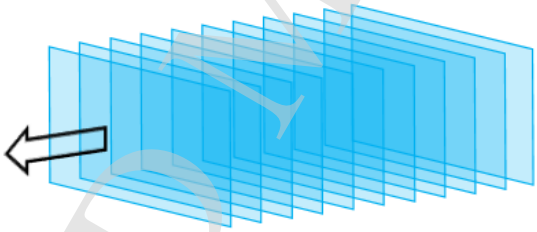

Fig. 1. 1D wave propagation.

In the 1D wave propagation theory, the effect of Poisson's ratio (lateral deformation) is not included in deriving the wave formula. As a consequence, the wave behavior can be dominated by the original condition. Although the infinite medium is considered in this theory, the transmission and reflection are able to happen in the presence of the material interface. Since this type of boundary condition just exists in the wave transmission direction, only the magnitude rather than the velocity of the wave will be changed. Accordingly, in the conventional GW-based NDE methods, the velocity of the wave is generally supposed as the constant value in the transmission media.[11]

On the other side, if the transmission medium is finite such as cylinder or plate structures, the mechanical variable will be imposed by the boundary condition including strain and stress constraints. In this case, when the wave transmits through the media, the reflection waves will be generated due to the boundary, and the direction and type of the wave will be changed. This type of wave is also called GW,[18,19] and the propagation comparison between traditional 1D wave and GW in a plate structure is demonstrated in Fig. 2.

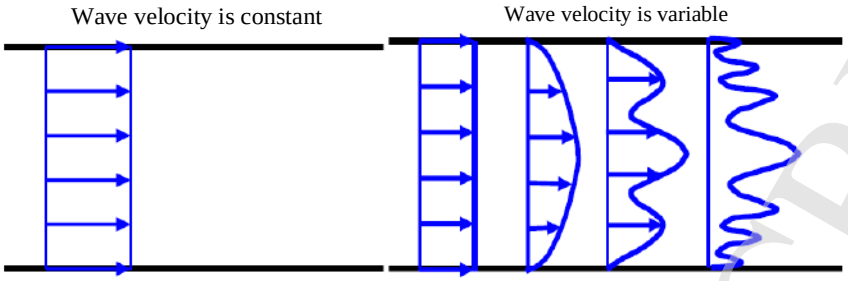

(a) (b)

Fig. 2. Wave propagation comparison between (a) 1D wave and (2) GW in a plate structure.

The GWs are capable of propagating in any finite medium including inelastic and elastic materials.[18] In the elastic material, the wave propagation follows the elastic theory,[20] while in the inelastic material the wave transmission employs the constitutive law of viscoelasticity. In Ref. 21, the control equation set and corresponding solution of GW propagating in the cylinder elastic structure with isotropic material properties have been developed according to the elastic theory, which considers the soil effect. In this study, the influences of different parameters including material property, geometric information of the structure, frequency, soil property and boundary condition on the GW propagation were investigated. The solutions calculated by the equation set are wavenumbers and angular frequencies. The dispersion relation is defined as the relation between real parts of frequency and wavenumbers. Through deriving the dispersion relation, the group velocity and phase velocity can be obtained,[21,22] shown as follows:

$$V_{gv} = \frac{w}{Re(\eta)'} \tag{1}$$

$$V_{pv} = \frac{w}{Re(d\eta)'} \tag{2}$$

where V_{gv} and V_{pv} denote the group velocity and phase velocity, respectively; w denotes the angular frequency; η denotes the wavenumber. Here, the spectrum relation is defined as the relation between frequency and wave velocity.

Since the wood is a type of orthotropic material, which should be considered as dispersion relation solution. The influences of different properties on wave propagation in the wood cylinder poles with both orthotropic and isotropic material properties have been studied in Ref.22, where the properties of isotropic wood material are set as: the modulus of elasticity is 23 GPa, density is 950 kg/m^3, and Poisson's ratio is 0.3. The properties of orthotropic wood material are given in Table 1.

Table 1 Material properties of orthotropic wood

Elastic modulus (GPa)			Shear modulus (GPa)			Elastic modulus (GPa)		
TD	RD	LD	RT	RL	TL	RT	RL	TL
0.85	1.955	23	0.357	1.513	1.037	0.682	0.044	0.023

Note: RT denotes radial transversal, RL denotes radial longitudinal, TL denotes transversal longitudinal, TD denotes transversal direction, RD denotes radial direction and LD denotes longitudinal direction.

Fig. 3 shows the relationships between wave phase velocity and frequency of wood cylinder poles with different material properties, in which the solid line represents the longitudinal wave and the dotted line denotes the flexural wave. We can see from Fig. 3 that for the isotropic material case when the frequency is below 5 kHz, both longitudinal and flexural waves have one branch. In this frequency range, the velocity of longitudinal wave is higher than that of flexural wave. When the frequency is increased to 15 kHz, there are three flexural wave branches and two longitudinal wave branches. On the other side, for the orthotropic material case, seven flexural wave branches and three longitudinal wave branches appear in the frequency of 10 kHz, which indicates that the longitudinal wave is not prominent. Accordingly, the dispersion characteristics of GW propagating in the wood utility pole bring the complexity and difficulty in processing the wave signals for accurate assessment of health condition. Aiming at fixing this problem, a novel NDE framework with advanced signal processing and artificial intelligence (AI) techniques is proposed in this study and will be presented in details in the following sections.

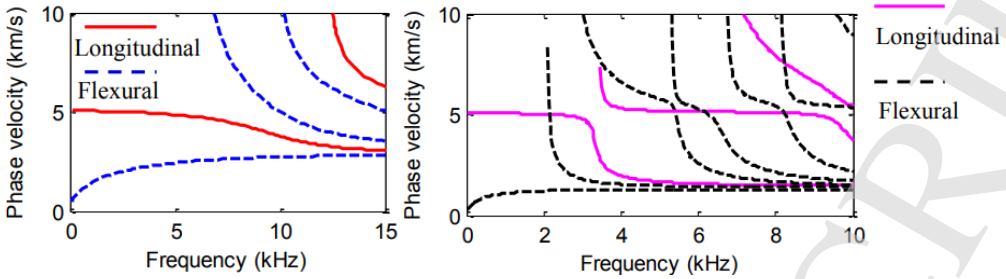

(a) (b)

Fig. 3. Phase velocity curves of wood cylinder poles with (a) isotropic and (b) orthotropic material properties.

3. Methodology

This study proposes a GW-based approach that can accurately and real-timely diagnose the health condition of in-service wood electricity poles. To begin with, the correlation coefficient-based EMD is utilized to decompose the wave signals captured from a portable multi-sensing system, and the energy information at each instantaneous frequency of the signal is extracted as the signal feature. Then, a feature vector is developed via combing the energy features from different sensors as the input of the diagnosis models. To avoid the redundancy of the features from different sensors and influences from external noises, the PCA is employed to select the optimal inputs for the diagnosis models. Finally, the machine learning techniques are used to develop the diagnosis models based the feature vectors and real condition of the poles.

3.1.GW feature extraction based on modified EMD

3.1.1. Overview of EMD

EMD was originally put forward by Huang, which is used to realize the adaptive signal decomposing.[23]The essence of the EMD is a self-adaptive stationary signal processing method. Currently it is the commonly used approach to extract the tendency and mean value of data sequence, which has been widely applied in the fields of fault diagnosis and structural monitoring.

The principle of the EMD is to decompose the complicated signal into several intrinsic mode functions(IMF) with different instantaneous frequencies and a residue.[24,25]In the EMD, the following assumptions are considered:

1) The data sequence of the original signal has at least two extremes, i.e. one maximum and one minimum.

2) The local time-domain characteristics of data sequence of the original signal are uniquely determined by the time scales between extreme points.

3) If the data sequence of original signal does not have extreme point but inflection point, the extreme can be obtained by one or more times of data differentiation, and then the decomposition result can be gained by the integration. Essentially, the IMFs can be obtained based on the time scale of data characteristic, and then the data sequence is decomposed.

The basic idea of the 1-dimentional EMD can be summarized as follows. First of all, he local maximum and local minimum points of the signal are extracted. Second, the curve interpolation is applied to the extreme points to obtain the upper envelope, the lower envelope and the mean envelope of the signal. Then, the signal that meets the condition of IMF will be filtered out sequentially using filtering algorithm. Finally, a signal is decomposed into several IMFs with decreasing frequencies and a residue. In each filtering process, an IMF is extracted, and the remaining signal will be filtered again. After all the filtering process, the original signal can be expressed as follows:

$$x(t) = r_n(t) + \sum_{i=1}^{n} c_i(t) \tag{3}$$

where $x(t)$ denotes the raw signal, $r_n(t)$ denotes the residue, and $c_i(t)$ denotes ith IMF.

To sum up, the procedure of the EMD is composed of the following steps:

Step 1.Calculate all the local maximum and minimum points of original signal.

Step 2. The upper envelop $x_{max}(t)$ and lower envelope$x_{min}(t)$ are obtained by fitting the extreme points based on cubic spline interpolation method, with the following relationship:

$$x_{min}(t) \le x(t) \le x_{max}(t) \tag{4}$$

Step 3.The mean values of the upperenvelop $x_{max}(t)$ and lower envelope$x_{min}(t)$ are obtained using Eq. (5):

$$m_{1l}(t) = \frac{x_{max}(t) + x_{min}(t)}{2} \tag{5}$$

Step 4. Extract the local detail information $h_{1l}(t)$ based on Eq. (6):

$$h_{1l}(t) = x(t) - m_{1l}(t) \tag{6}$$

Step 5. Check whether $h_{1l}(t)$ meets the condition of IMF. If so, it is the first IMF separated from original signal, i.e. $c_1(t) = h_{1l}(t)$; otherwise, $h_{1l}(t)$ is regarded as original signal, and repeat Steps (1)–(5) until the following condition is satisfied:

$$h_{1(k-1)} - m_{1k}(t) = h_{1k}(t) \tag{7}$$

where $m_{1k}(t)$ denotes the mean value of upper and lower envelopes. Since $h_{1k}(t)$ meets the definition of IMF, the expression of $c_1(t)$ is shown as follows:

$$c_1(t) = h_{1k}(t) = x(t) - \sum_{i=1}^{k} m_{1i}(t) \tag{8}$$

where $h_{1k}(t)$ is the first IMF extracted from original signal. The remaining signal can be expressed as follows:

$$r_1(t) = x(t) - c_1(t) \tag{9}$$

Step 6. $r_1(t)$ is regarded as original signal and repeat above steps. Accordingly, $c_2(t)$, $c_3(t)$, …, $c_n(t)$ can be obtained, shown as follows:

$$c_n(t) = r_{n-1}(t) - r_n(t) \tag{10}$$

where $r_n(t)$is the residue which represents the tendency of original signal. At this point, the decomposition of original signal using EMD is finished and original signal can be represented by Eq. (11).

$$x(t) = \sum_{i=1}^{n} c_i(t) + r_n(t) \tag{11}$$

To sum up, the flowchart of the EMD algorithm is illustrated in Fig. 4.

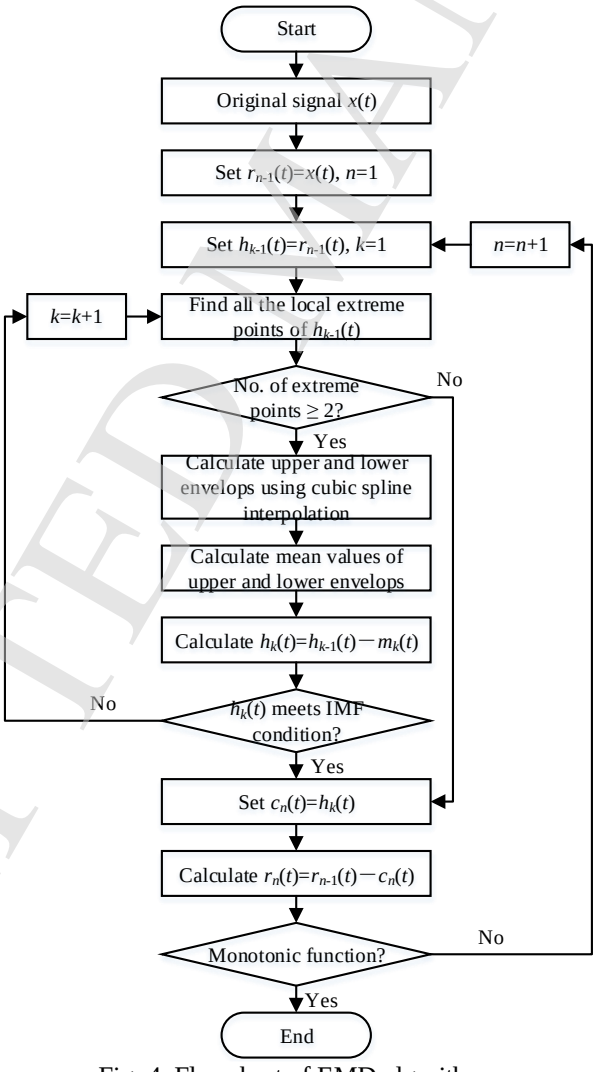

Fig. 4. Flowchart of EMD algorithm.

3.1.2. Modified EMD

Even though the EMD method has a promising prospect in processing nonlinear and nonstationary signals, the decomposition results may be inaccurate sometimes due to the problem of mode mixing.[26,27]After the signal is decomposed using the EMD, the obtained one or more IMFs contain different time scales. This phenomenon is called mode mixing. The main reasons contributing to this problem can be summarized in threefold. First of all, the actual signal often contains the noise, which can be considered as the high-frequency component and lead to the mode mixing accordingly.Secondly, in the real situation, the low sampling frequency may lead to the omission of several extreme points. In this case, the obtained IMFs have obvious deviations from that of real signals, and the accumulation of these deviations will cause the mode mixing. Last but not least, in EMD the cubic spline interpolation method itselfhas the iteration error, which indicates that the obtained IMFs have prediction errors compared to the real frequency components in the signal. In the same way, the summation of the error in each spline interpolation may result in the mode mixing. As a whole, the problem of mode mixing has seriously hindered the development of EMD, which may have serious defects in the application of modal parameter identification, fault diagnosis, etc.

In this study, to avoid the pseudo IMFs due to the mode mixing, a modified EMD (MEMD) method is proposed to process the acquired GW signals. Since in the practice it is impossible to know the number of the IMFs in the original signal in advance, a quantitative judgment is necessary to check whether the extracted IMF is pseudo or not. Generally, if the obtained IMF is indeed the modal component contained in the signal itself, there exists a certain correlation between this IMF and original signal. On the contrary, if it is a pseudo IMF, the correlation between this IMF and original signal should be lower. Based on this idea, the correlation coefficients between IMFs obtained from original signal by EMD and the original signal are proposed in this study to evaluatethe authenticity of the IMFs, the mathematical expression of which is shown in Eq. (12):

$$\tau_i = \frac{N\sum_{t=1}^{N} x(t) imf_i(t) - \sum_{t=1}^{N} x(t) \sum_{j=1}^{N} imf_i(t)}{\sqrt{[N\sum_{t=1}^{N}[x(t)]^2 - [\sum_{t=1}^{N} x(t)]^2][N\sum_{t=1}^{N}[imf_i(t)]^2 - [\sum_{t=1}^{N} imf_i(t)]^2]}} \tag{12}$$

where N denotes sampling number of the signal, $x(t)$ denotes original signal, and $imf_i(t)$ denotes ith IMF obtained from $x(t)$. When the MEMD method is used to process the SW signals for health condition diagnosis of wood electricity poles, a threshold should be set in advance. The IMFs with the values smaller than this threshold demonstrate the inessential contributions to the extraction of signal patterns, which should be discarded and added to the residue directly. Eventually, the IMFs with the values higher than this threshold are retained as signal features for optimal selection.

3.1.3. Performance verification of MEMD

To verify the performance of the proposed MEMD and illustrate its superiority, a comparative investigation is carried out in this subsection through the comparison of decomposition results of a simulated signal using EMD and MEMD. In this investigation, the signal$S(t)$ is simulated based on superposition of sinusoidal waves and constant term with the mathematical expression in Eq. (13):

$$S(t) = 2 + 0.3\sin\left(2\pi f_1 t + \frac{\pi}{6}\right) + 0.5\sin\left(2\pi f_2 t + \frac{\pi}{3}\right), \qquad f_1 = 2.5Hz, \qquad f_2 = 6Hz \tag{13}$$

where t denotes the point-in-time. In this simulation, the sampling interval is 0.001 s and the sampling duration is 5 s.

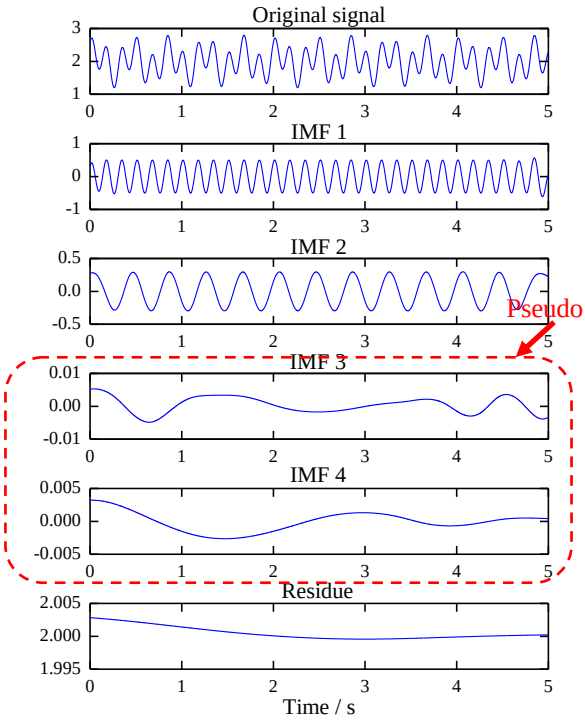

Fig. 5. Verification result of EMD based on the signal without any noise.

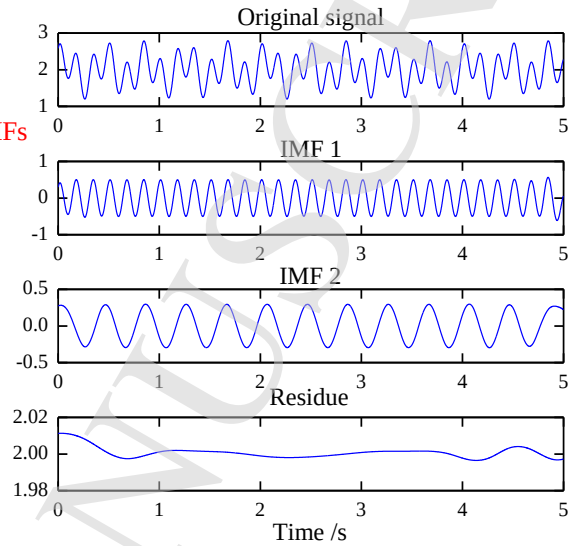

Fig. 6. Verification result of MEMD based on the signal without any noise.

To begin with, the EMD method is employed to decompose this simulated signal, and the decomposition result is displayed in Fig. 5. According to the steps in Section 3.1.1, the first IMF (denoted by IMF1) is extracted first, followed by IMF2, IMF3 and IMF4. Finally, the residual part is regarded as the residue of the original signal. Therefore, it is clearly seen from the figure that in this decomposition, four IMFs are obtained from the original signal. However, it is noticeable that the original signal only has two frequency components corresponding to 2.5 Hz and 6 Hz, respectively, which indicates that two pseudo IMFs exist in the decomposition result. Then, MEMD is used to process the same signal to check its performance. In this work, the threshold value is set at 0.3, which means that the IMFs with the correlation coefficients between them and original signal higher than 0.3 will be maintained and the IMFs with the correlation coefficients lower than 0.3 are considered as pseudo IMFs and added to the residue. Fig. 6 portrays the decomposition result using MEMD method. It is apparent that only IMF 1 and IMF 2 are maintained as the effective components, corresponding to the frequency components of 2.5 Hz and 6 Hz in the original signal. The correlation coefficients between first two IMFs and original signal are 0.8622 and 0.5081, respectively, which satisfies the threshold condition. The IMF 3 and IMF 4, however, are discarded, since their correlation coefficients with the original signal are 0.0112 and 0.0278, respectively, which are lower than the threshold value. Accordingly, the proposed MEDM method has better performance in signal decomposition than the EMD method, which can effectively eliminate the influence of pseudo IMFs.

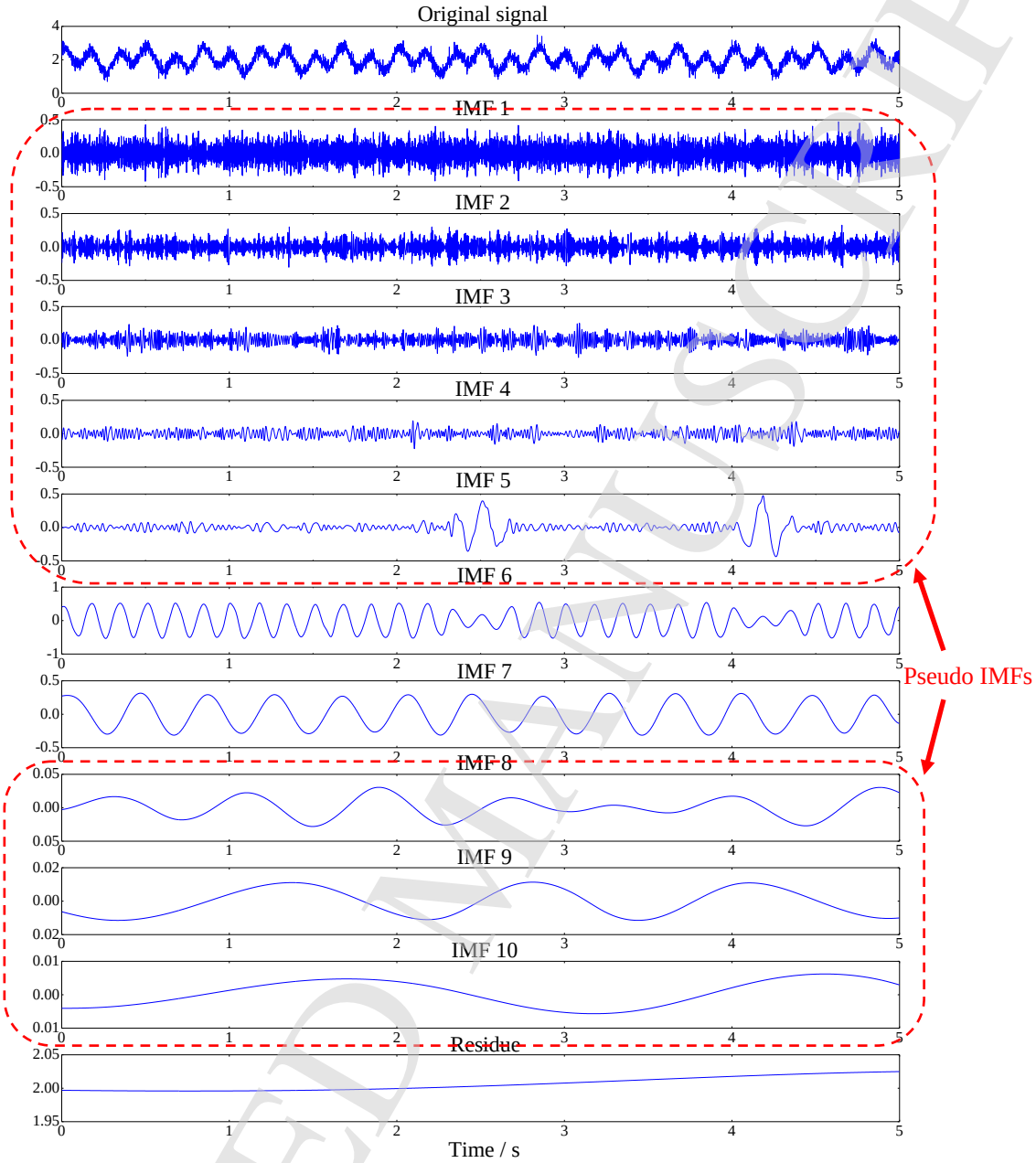

Fig. 7. Verification result of EMD based on the noisy signal.

In the practice, the signals measured in the field are always pullulated with the noises, which can lead to the mode mixing problem as mentioned in Section 3.1.1. Hence, further verification of the capacity of the proposed MEDM method to decompose the noisy data is necessary, before it is adopted to process the GW signals to diagnose the health condition of wood utility pole in this study. Here, the 20dB signal-to-noise ratio (SNR) Gaussian white noise is added into original signal to simulate the noisy data measured in the field. Then, both EMD and MEMD are utilized to decompose the noisy signal, the results of which are displayed in Fig. 7 and Fig. 8. It is clearly seen from Fig. 7 that there are ten IMFs extracted from the noisy signal using EMD method, in which IMFs 1-5 and IMFs 8-10 are pseudo IMFs. Obviously, the IMFs 1–5 are high-frequency components, which are mainly caused by random noises. The correlation coefficients between IMFs 1-10 and noisy signal are 0.3214, 0.1877, 0.1347, 0.1013, 0.2265, 0.7483, 0.4593, 0.0150, 0.0121 and -0.0042, respectively. According to the threshold requirement, IMF 6 and IMF 7 are selected as effective IMFs in the signal decomposition, the results of which are depicted in Fig. 8. As a consequence, it can be concluded that the developed MEDM outperforms the EMD in avoiding the pseudo IMFs decomposed from noisy signals.

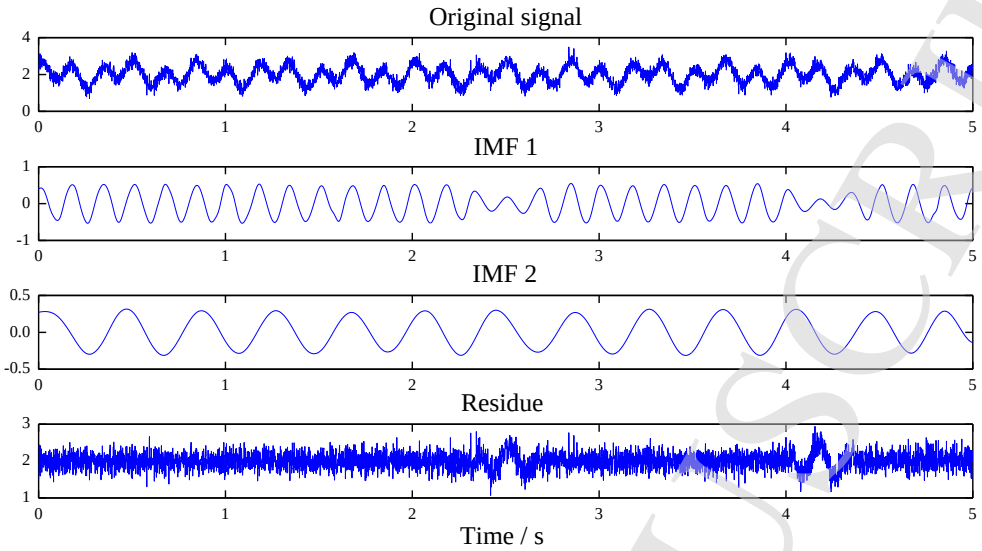

Fig. 8. Verification result of MEMD based on the noisy signal.

3.1.4. Energy feature extraction based on MEMD

After the acquired GW signals are decomposed by the MEMD method, the obtained IMFs are capable of describing a range of stationary signals on the characteristic dimension, which contain unique energy information. In this research, first few IMFs are employed to calculate the energy ratio (*R*), which is used as feature index to reflect the health pattern of the GW signals. The relevant equations for calculating the energy ratio are provided as follows:

$$E_k = \sum_{t=1}^{N_w} |c_k(t)|^2 \tag{14}$$

$$R_k = \frac{E_k}{\sum_{k=1}^{j} E_k} \tag{15}$$

where E_k denotes the signal energy of *k*th IMF andN_w denotes the length of GW signal. Generally, the structural damage or crack may cause the change of structural natural frequencies, which can be reflected in thevariations of the GW signal's energy distributions compared with that of the intact structure without any damage or crack. Hence, the proposed IMF energy ratio can be considered as an effective indicator to diagnose the health status of electricity poles. Due to simultaneous presence of various wave modes, it is unlikely to use only one sensor to accurately capture the complicated behaviour of GW for pole health diagnosis in this study. Accordingly, the multi-sensing approachisadopted to collect GW signals from different sensors. However, how to effectively combine the energy feature gained from different sensors is a challenging issue. In this work, the real-coded approach is adopted to develop a feature vector via integrating IMF energy ratios one after another, the schematic of which is shown in Fig. 9.

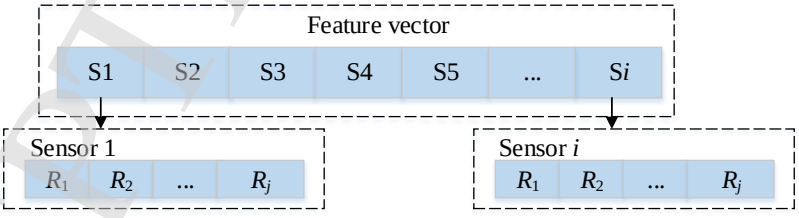

Fig. 9. Feature vector development

3.2. Optimal feature selection based on PCA

The feature vector of energy ratio obtained from multiple sensors will include sufficient information about signal pattern related to the pole condition. However, occasionally the extracted features may be inaccurate or contaminated by the harmful noises due to a variety of disturbances in the field. In addition, signal patterns captured from different sensors are redundant sometimes. In this case, the generalization ability of the evaluation model will be affected if the feature vector is employed directly as the model inputs for training. To fix this problem, the PCA is utilized in this study to deal with the feature vector, which is one of most powerful

data compression and feature extraction techniques for processing high-dimensional data. Via the projection, it is able to transform the high-dimensional signal features into low-dimensional space with as little information loss as possible, which reduces the signal feature dimension and simplifies the structure of feature vector accordingly. On the other hand, the PCA can also be used to get rid of harmful noise.[28,29] Because of the random property, the noise can be represented by less important principal components (PC).By disregarding the PCs with lower orders, the effect of noises on the feature vector will be eliminated accordingly.

In this work, the feature vector of the GW signals captured from i sensors can be expressed as $R=[R_1,R_2,\ldots,R_p]$ ($p=i\cdot j$), where j denotes the number of IMF energy ratios of GW in one sensor. The linear combinations of all the elements (R_1, R_2, …, R_p) in the feature vector can be expressed as follows:

$$\begin{aligned} PC_1 &= a_{11}R_1 + a_{12}R_2 + \cdots + a_{1p}R_p \\ PC_2 &= a_{21}R_1 + a_{22}R_2 + \cdots + a_{2p}R_p \\ &\vdots \\ PC_p &= a_{p1}R_1 + a_{p2}R_2 + \cdots + a_{pp}R_p \end{aligned} \tag{16}$$

where $a_{i1} + a_{i2} + \cdots + a_{ip} = 1\ (i = 1, \ldots, p)$; there is no correlation between arbitrary two elements in the feature vectorR_m and R_n ($m\neq n$, $m,n=1,2,\ldots,p$); PC_1 has the largest variance among all the linear combinations of the elements in the feature vector R; PC_2 has the largest variance among all the linear combinations of the elements in the feature vector R that are not related to PC_1; The sum of variances of PC_1, PC_2, …, PC_p is equal to that of R_1, R_2, …, R_p. Hence, the essence of the PCA to select optimal features for the condition diagnosis of wood poles can be regarded as solving the transfer matrix $A = \begin{bmatrix} a_{11} & \cdots & a_{1p} \\ \vdots & \ddots & \vdots \\ a_{p1} & \cdots & a_{pp} \end{bmatrix}$, which can be divided into the following steps.

Step 1. Normalize the IMF energy ratios in the feature vector, and calculate the covariance matrix of the energy ratios.

Step 2. Calculate the eigenvalue of the covariance matrix, i.e. $\lambda_1\geq\lambda_2\geq\ldots\geq\lambda_p$. The corresponding unit eigenvectors are T_1, T_2, …, T_p. The transfer matrix A is the transposed matrix of unit eigenvector, i.e. $A = T'$, where the ith row in A corresponds to the unit eigenvector of ith eigenvalueλ_i. The variance of ith PC (PC_i) isequal to ith eigenvalue of the covariance matrix.

Step 3. Calculate the individual variance contribution of kth PC (PC_k) using Eq. (17)

$$\eta_k = \frac{\lambda_k}{\sum_{k=1}^{p}\lambda_k} \tag{17}$$

If the first l ($l<p$) PCs are considered, the accumulated contribution of PC_1, PC_2, …, PC_pcan be expressed as follows.

$$\xi_l = \frac{\sum_{k=1}^{l}\lambda_k}{\sum_{k=1}^{p}\lambda_p} \tag{18}$$

Step 4. Select the PCs according to the accumulated variance contribution, and the dimension of feature vector is greatly reduced.

3.3. Condition diagnosis based on machine learning techniques

The condition diagnosis of wood utility poles can be regarded as dealing with the problem of binary pattern recognition, where an accurate and robust diagnosis model is required. In this study, the machine learning (ML) techniques are selected to build up the prediction model for diagnosing the pole condition. The model inputs are the optimal features (first few PCs) selected from the feature vector of IMF energy ratios while the model output is the pole condition, i.e. intact or damaged. Here, three different ML approaches, classification and regression (CART),k-nearest neighbours (k-NN)and support vector machine (SVM) are chosen, the principles of which are described in the following parts.

3.3.1. CART

The CART, first presented by Breinman et al., is based on the minimization criterion of Gini index value.[30] Compared with commonly used Iterative Dichotomiser 3 (ID3) decision tree learning, the CART has faster calculation speed and better stability, which is able to support the multiple segmentations of continuous feature data. Compared with other types of machine learning algorithms such as logistic regression (LR), artificial neural networks (ANN), etc, the CART does not need to establish a nonlinear model, and can intuitively make the decision for classification and extract knowledge rules based on decision tree graph.[31]

The main mechnism of the CART could be concluded as following. Suppose that the class number is *Mc* and the probability of the sample belong to *mc*th class is p_{mc}. The Gini index of probability distribution of this sample can be expressed as follows:

$$\mathrm{Gini}(p) = \sum_{mc=1}^{Mc} p_{mc}(1-p_{mc}) = 1 - \sum_{mc=1}^{Mc} {p_{mc}}^2 \quad (19)$$

The Gini index of sample set *DS* can be expressed by:

$$\mathrm{Gini}(DS) = 1 - \sum_{mc=1}^{Mc} \left(\frac{|C_{mc}|}{|DS|}\right)^2 \quad (20)$$

where $|DS|$ denotes total sample number of set *DS*; $|C_m|$ denotes the number of sample subset belonging to *mc*th class in the set *DS*; Gini index Gini(*DS*) denote the uncertainty of the set *DS*.

In the set *DS*, the samples with the value of attribute *A* equal to *a* form the subset *DS*1, while the rest samples form the subset *DS*2. The Gini index of the set *DS* under the condition of attribute *A* can be expressed by:

$$\mathrm{Gini}(DS, A) = \frac{|DS1|}{|DS|}\mathrm{Gini}(DS1) + \frac{|DS2|}{|DS|}\mathrm{Gini}(DS2) \quad (21)$$

The greater the Gini index, the greater the uncertainty of the sample set, which is similar to the information entropy. Accordingly, it can be employed as the index to divide the sample set.

3.3.2. *k*-NN

The *k*-NN algorithm was developed to classify the unknown data based on existing data with known labels.[32]The essence of *k*-NN is analogy learning, that is learning by comparing the given test sample with training samples. Suppose that in the last section, *l* PCs are selected from feature vector of IMF energy ratios as the inputs of the ML model, which indicates that all the training samples should be in this *l*-dimensional space. When an unknown test sample is given, the *k*-NN algorithm searches the *l*-dimensional pattern space and finds *k* training samples that are closest to the unknown test sample. These *k* training samples can be regarded as *k* nearest neighbours of unknown sample.

The implementation of *k*-NN is based on the following assumptions: (1) all the data and labels belong to the numeric types; (2) the smaller the distance between two samples, the more similar these two samples; (3) each attribute (PC) has equal weight; (4) attribute values are normalized; (5) if one attribute value of sample x_1 and (or) sample x_2 are lost, their distance are supposed to be maximum possible distance. Here, Euclidean distance is employed to measure the similarity between test sample$S_i$and training sampleS_j, the expression of which is shown in Eq. (19):

$$dist(S_i, S_j) = \sqrt{\sum_{k=1}^{l} (S_{i,k} - S_{j,k})^2} \quad (22)$$

The membership degree of test sample S_i belonging to the class C_j is defined as follows:

$$MD(S_i, C_t) = \sum_{S_j \epsilon kNN(S_i)} dist(S_i, S_j)\delta(S_j, C_t) \quad (23)$$

where *k*-NN(S_i) denotes the nearest neighbour set; $\delta(S_j,C_t)$ denotes the class attribute of S_j belonging to C_t, i.e. $\delta(S_j, C_t) = \begin{cases} 1, & S_j \epsilon C_t \\ 0, & other \end{cases}$.

Therefore, identifying the class of $S_i$is considered as calculating an optimization problem as follows:

$$C\ arg\ maxMD(S_i, C_t) \quad (24)$$

The class *C* with maximum membership degree should be the class of S_i.

3.3.3. SVM

SVM is a commonly used machine learning method based on statistical learning theory, which has the advantages for solving the nonlinear pattern recognition problems with small sample.[33] The mechanism of SVM is to learn and improve the generalization capacity by search for the structural risk minimization. Essentially, it can be transformed into a convex quadratic optimization problem. Suppose there is a data set $T=\{(x_1,y_1),\ldots,(x_i,y_i),\ldots,(x_l,y_l)\}$. Based on the nonlinear function, the input data can be mapped into the high-dimensional space for regression, shown in Eq. (25):

$$f(x_i) = w \cdot \varphi(x_i) + b \quad (25)$$

where l denotes the sample number; b denotes the bias; w denotes the weight vector; $\varphi(x_i)$ denotes the kernel function, which is used to transform the linear problem into nonlinear problem. In this work, the radial basis function (RBF) is chosen as the kernel with the following expression:

$$\varphi(x_i) = e^{-\frac{\|x_i - x\|^2}{2\sigma^2}} \tag{26}$$

where σ denotes the kernel parameter. The target of the SVM is to find an optimal hyperplane to separate two categories of data, which can be transformed into the following optimization problem with the constraints.

$$\min \phi(w) = \frac{1}{2}\|w\|^2 \quad s.t.\ y_i[(w \cdot \varphi(x_i) + b)] \geq 1\ (i = 1,2, \dots, l) \tag{27}$$

Sometimes the samples cannot be well classified and the classification errors exist in the developed SVM models. In this case, a slack variable is added into the constraints to solve the error problem, shown as:

$$y_i[(w \cdot \varphi(x_i) + b)] \geq 1 - \xi_i (i = 1,2, \dots, l) \tag{28}$$

When $0 < \xi_i < 1$, all the samples can be correctly classified. When $\xi_i \geq 1$, x_i will be misclassified. To avoid this problem, the penalty term $C\sum_{i=1}^{l}\xi_i$ is added to the minimization target and the fitness function can be written as follows:

$$\phi(w, \xi) = \frac{1}{2}\|w\|^2 + C\sum_{i=1}^{l}\xi_i \tag{29}$$

Therefore, combine Eq. (28) and Eq. (29), and the optimization problem with the constraints can be expressed as:

$$\min \phi(w, \xi) = \frac{1}{2}\|w\|^2 + C\sum_{i=1}^{l}\xi_i \quad s.t.\ y_i[(w \cdot \varphi(x_i) + b)] \geq 1 - \xi_i (i = 1,2, \dots, l) \tag{30}$$

where $\sum_{i=1}^{l}\xi_i$ denotes the upper bound of the misclassified sample number, which is used to measure the deviation degree of the data from ideal partition condition. C denotes the penalty coefficient. To calculate this optimization problem, the Lagrange function is employed to transform the optimal classification problem into its dual form, shown as:

$$\begin{aligned} &\max L(\alpha) = \sum_{i=1}^{l}\alpha_i - \frac{1}{2}\sum_{i=1}^{l}\sum_{j=1}^{l}\alpha_i\alpha_j y_i y_j \varphi(x_i, x_j) \\ &s.t.\ 0 \leq \alpha_i, \alpha_j \leq C\ (i, j = 1,2, \dots, l), \qquad \sum_{i=1}^{l} y_i\alpha_i = 0 \end{aligned} \tag{31}$$

Hence, the corresponding classification decision function of SVM can be expressed in Eq. (32).

$$f(x) = sgn\left(\sum_{i=1}^{l}\alpha_i y_i \varphi(x_i, x) + b\right) \tag{32}$$

In SVM, the penalty coefficient C and kernel factor are two main parameters that are capable ofremarkably affecting the performance of the model. In this research, the values of C and $\sigma^2$are set as 30 and 2, respectively, according to the suggestions in Ref. 34.

4. Field test validation and results analysis

4.1. Field test of electricity poles

To evaluate the performance of the proposed NDE framework for condition diagnosis of wood utility polein field, a number of tests have been conducted on 39 wood utility poles in the pole yard at Mason Park, New South Wales, Australia, as shown in Fig. 10.These poles are composed of 15 new poles (No. 1-15) and 24 decommissioned poles (No. 16-39) with various health conditions. The pole species is Ironbark, Grey and all the poles were treated by copper chrome arsenate (CCA). The diameter of the poles ranges from 0.2 m to 0.27m, while the embedded depth of the poles is between 1.45 m and 2 m. For the convenience of pole testing in field, a portable NDE device with the feature of multi-sensing was developed, which is composed of a sensor bar with seven integrated circulated piezoelectric (IPC) accelerometers, an impact hammer, two USB chassis, two 4-channel data acquisition (DAQ) modules and a laptop for the operation and data management. Fig. 11 shows the hardware makeup and software interface of the multi-sensing system, respectively.The impact hammer is a PCB 086D05 model with 1 mV/lbf sensitivity. The sensor is the ceramic shear ICP accelerometer of 352C34 model with 100 mV/g sensitivity and 0.5 Hz to 10 kHz frequency bandwidth. The DAQ system consists of two 4-channel modules of 9234 model incorporated in USB chassis of cDAQ-9171 model, thus the system has eight channels for data transmission, where the first channel is connected with the impact hammer and the remaining channels are connected to seven accelerometers. The sensor bar is designed to closely attach the accelerometers

to the surface of the tested pole. The spacing between two neighbouring accelerometers is 200 mm. The spacing between two neighbouring accelerometer is 200 mm and the location of the bottom accelerometer is 300 mm above the ground. The DAQ interface is designed based on the software LabVIEW, which can clearly show the time-domain waveforms collected from seven sensors. If the test results are not as good as expected, the operator can discard the test data and then redo the test to make sure good quality of collected data from electricity poles. To avoid the influence of moisture on the wave behaviour, all the tests were conducted in the clear and dry weather condition.

Fig. 10. 39 poles at the pole yard.

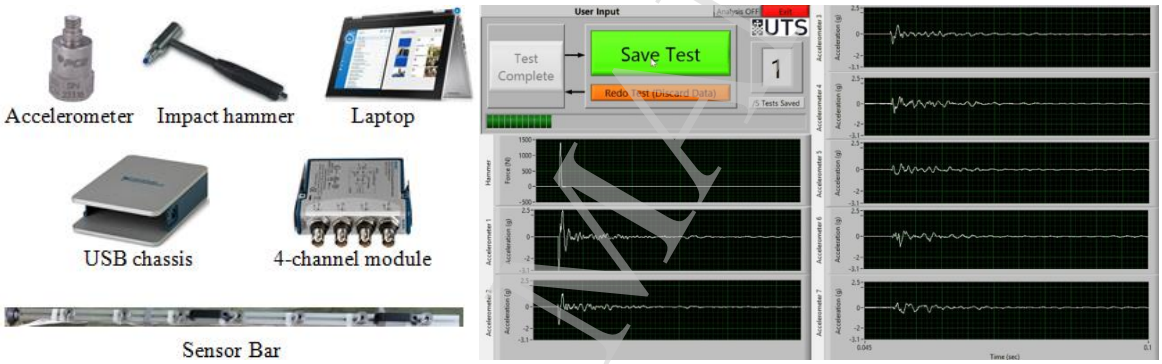

(a) Hardware makeup (b) Software interface

Fig. 11. Portable NDE device for pole testing.

Fig. 12 (a) demonstrates how the developed portable NDE device is employed by one operator for pole testing. The sampling frequency is set at 51.2 kHz with 0.5 s sampling duration. To evaluate the influence of excitation location on the diagnosis accuracy of health condition of the pole, three different excitation locations are selected for the NDE of the pole, i.e. front top (FT) at 1.8m height, back top (BT) at 1.8 m height and back bottom (BB) at 0.2 m height from the ground line, which are clearly indicated in Fig. 12 (a). To obtain enough test data for the development and validation of the diagnosis model of wood poles, the sensor bar is deployed at two random locations of the pole surface, denoted by L1 and L2, and five hammer impacts are implemented in the transversal directionfor each sensor bar location, which indicates 10 individual tests for each pole. Because the measurements from seven accelerometers can be obtained in the meantime for each individual test, there are 8190 groups of wave signals collected in total (39 poles × 3 excitation locations × 2 sensor bar locations × 5 hits × 7 accelerometers).After the testing of the poles, the health conditions of all the tested poles were examined by the experts according to their experiences and latest records of residual strengths of poles in data management system.The details are provided as follows. First of all, 24 decommissioned poles were removed from the soil and split into multiple small sections along the cross-section by the contractors using an electric motor saw. Then, the appearance and cross-section areas were photographed and analyzed in accordance with the severity of obvious damage and strength degradation, which is shown in Fig. 12 (b). Generally, the poles with minor damages and less than 30% strength deterioration are regarded as intact poles while the poles with medium or severe damage as well as more than 30% strength deterioration are deemed as damaged poles. Due to perfect strength capacity, 15 new poles are considered as intact poles directly without autopsy examination. Finally, the collected data together with corresponding pole condition scenarios are used to develop and validate the machine learning models for online health diagnosis of the poles in the field, which will be presented in the following section.

(a) (b)

Fig. 12. Pole testing and autopsy results.

4.2. Result analysis and discussion

To prevent the signal deviation due to different force strengths included by different operators, all the acquired wave signals were normalized according to the maximum values of force responses. Fig. 13 shows the time-domain GW signals of the seven accelerometers related to three impact locations. It can be noted here that these signals are related to the sensor bar location L1. From three sub-figures, the signals acquired from different impact locations and sensors have different have different waveforms. For instance, for different impact locations the sensor signals arrive at the trough first for the front top excitation, while the sensor signals reach the peaks first for the back top and bottom excitations. Additionally, for different sensor locations, the top sensor (S1) obtain the first peak or trough values earlier than the bottom sensor (S7) for the cases of front and back top excitations, while the bottom sensor gets the first extreme value earlier than the top sensor for the case of back bottom excitation. This shows that different impact locations will result in different wave behaviours, which should be processed separately for the model development and validation.

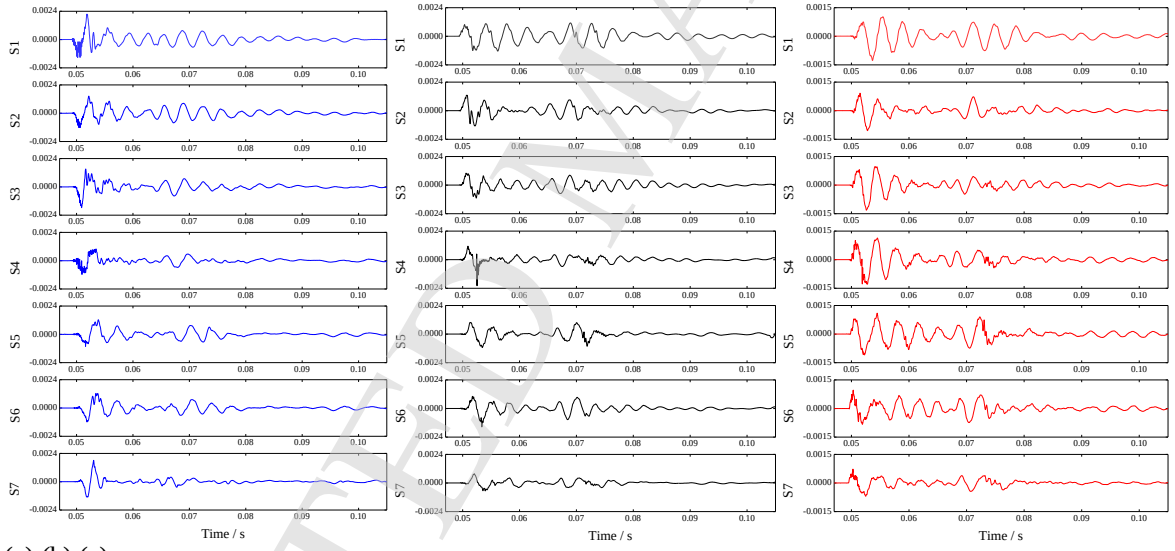

(a) (b) (c)

Fig.13. Example of GW signals captured from an intact poleat sensor bar location L1(a) front top excitation, (b) back top excitation and (c) back bottom excitation. (Signal unit: m/s^2)

Then, the developed MEMD method is implemented to decompose the GW signals and extract the IMF energy features. The threshold of the correlation coefficient is also set as 0.3. Fig. 14 presents the example of decomposition results of the acquired GW signals of an intact pole from back top excitation. It is observed from the figure that the original GW signals are decomposed into three IMFs and a residue. The correlation coefficients between three IMFs and original signal are 0.9049, 0.5017 and 0.3502, respectively, which satisfies the threshold condition. In this study, the first three IMFs are employed to construct the feature vector, even if more than three IMFs can be extracted for some GW signals. Since there are seven accelerometers in the multi-sensing device, the dimension of the developed feature vector should be 21 (3×7). If all the elements in feature vector are directly employed as inputs of machine learning models, the models will consider too much local information of features, which may result in the over-fitting problem of the trained models. The main reason resulting in this problem is that the developed model is heavily dependent on the training samples. The models will remember almost all the data features, including too many local features and false features caused by the

noise. The over-fitted model will provide inaccurate prediction results for new data excluded in the training samples, and result in the poor performance in the application. To fix this problem, the feature vectors of all the samples are dealt with by PCA to select optimal featuresfor the dimension reduction. After the operation, the 21 elements in the feature vector are mapped into 21 PCs, which are obtained via the linear combinations of original feature elements. These PCs are orthogonal to each other and arranged according to their contributions to feature information. Fig. 15 shows the PCA results of feature vector with IMF energy ratios, including both individual and accumulative contributions of first 15 components to entire feature information. It is clearly seen that first 10 PCs can contain almost 95% of the entire information in spite of excitation location. Accordingly, when the machine models are designed, first 10 PCs will be employed as the inputs to take the place of the feature vector with 12 elements. Even if 5% of energy features are missing, the input numbers of machine learning models are significantly decreased, which benefits the model training and avoids the over-fitting problem.

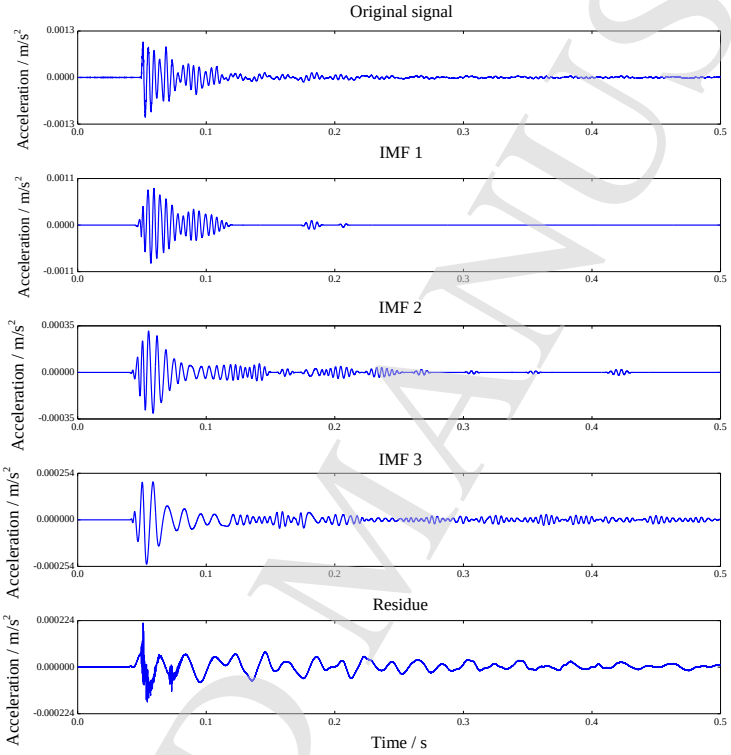

Fig. 14. Decomposition result of GW signal tested from an intact pole using MEMD.

To further elaborate the capacity of presented feature extraction selection methods in this study, the extracted first three PCs (PC1, PC2 and PC3) are plotted in the 3-D graphs to distinguish different types of health condition of wood electricity poles. The relevant results are displayed in Fig. 16 (a), (b) and (c), corresponding to different excitation locations, in which square blue points denote the intact samples and circular red points denote the damaged cases. It can be observed that most data samples are obviously separated according to first three PCs, even though a small amount of samples are overlapped. Compared with the front excitation, the back excitations have less overlapped areas between intact and damaged samples. Based on the classification results using first three PCs in Fig. 16, it is conceivable that 10 PCs can better diagnose the health status of electricity pole. As a consequence, the proposed feature extraction and selection based on MEMD and PCA have been proved to be effective in obtaining the damage-sensitive features for health diagnosis of wood poles.

In the real situation, it is necessary to obtain a model or classifier to automatically make the diagnosis of the pole heath condition based on the newly captured GW signals, which may be different from the signals in existing database. Here, three different machine learning approaches, CART, SVM and *k*-NN, are adopted to develop the diagnosis models. The implementation of machine learning algorithms is based on Matlab 2015a Classification Learner toolbox. Since different excitation locations will induce different wave propagation paths, three individual diagnosis models are developed corresponding to three excitation locations for each type of machine learning method. The model inputs are first 10 PCs captured from the feature vector while the model output is the health condition “0” or “1”, where “0” denotes the damaged pole and “1” denotes the intact pole. For each model, 390 (39 poles × 2 sensor bar locations) groups of data samples could be employed to train and validate the models. In this part, 10 fold cross-validation strategy is utilized for this task, the process of which are divided into three steps: 1) 390 groups of PCs are divided into ten sets averagely and randomly, which

indicates that there are 39 groups of data in each set; 2) of ten sets, one set of data is taken out as validation samples to evaluate the performances of the trained machine learning models, while the rest data (nine sets) are regarded as the training samples to build up the diagnosis models; 3) The training and validation process of the learning models is repeated ten times until all the data sets have been used as the validation samples; 4) The model performance is evaluated via averaging the validation results of ten sets of data. The main benefit of such kind of model evaluation is that the samples with different labels of health condition of wood poles are fully utilized for model development and evaluation, and each data sample can be used as the testing sample for model validation once.

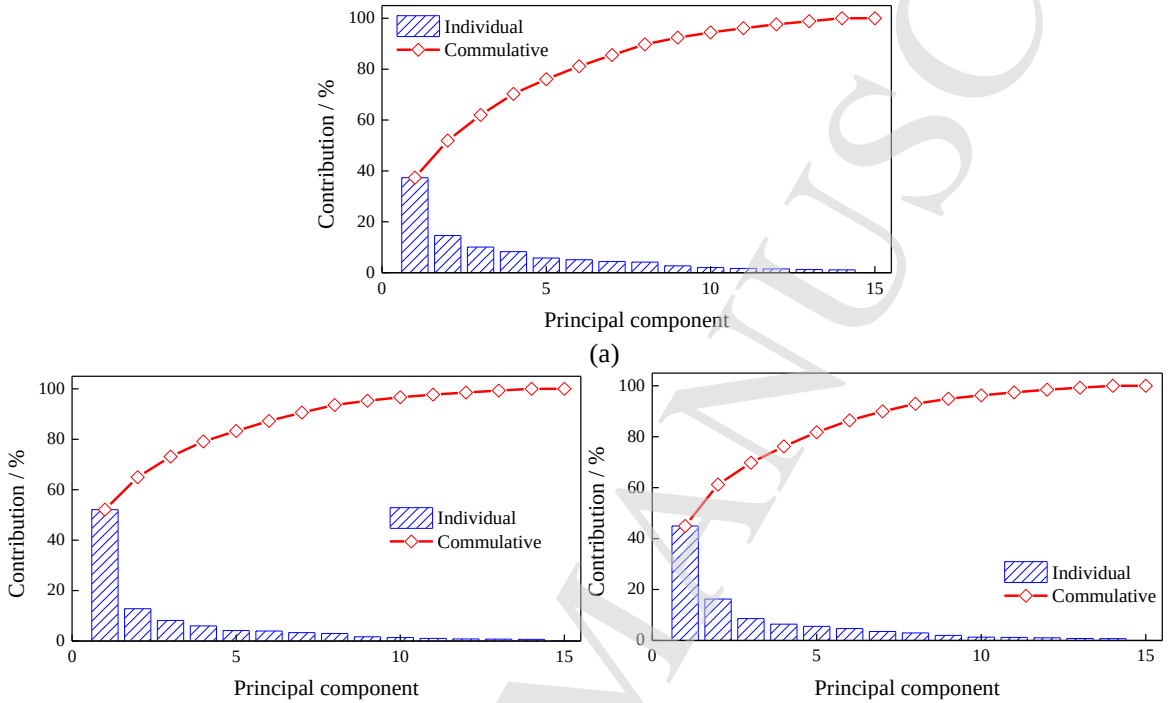

Fig. 15. PCA results of IMF energy feature vector: (a) front top excitation, (b) back top excitation and (c) back bottom excitation.

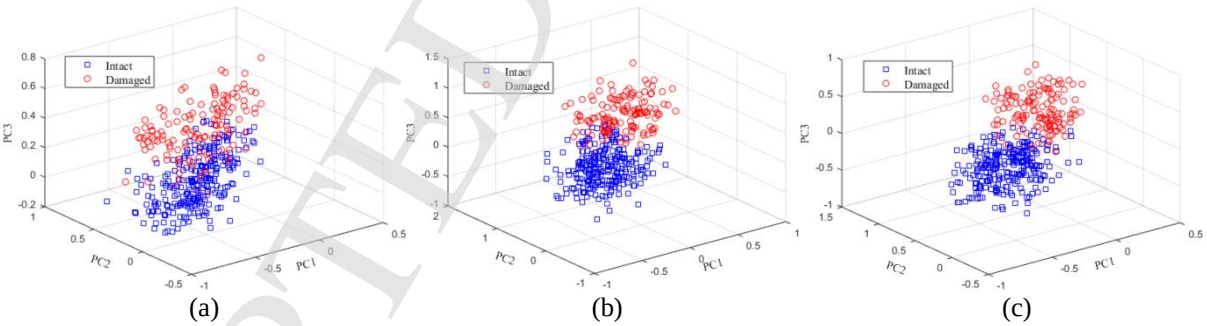

Fig. 16.Classification result of GW data based on first 3 PCs: (a) front top excitation, (b) back top excitation and (c) back bottom excitation.

The evaluation results of three machine learning models are shown in Figs. 17−19, where the confusion matrix is used to demonstrate the model accuracy in terms of reporting the numbers and percentages of false negative, false positive, true negative and true positive. The accuracies of models corresponding to different excitation locations are also displayed in Table 2. It can be observed from the figures that the prediction accuracies of all the models are above 82%, which is acceptable in machine learning study.Among three machine learning approaches, the SVM and *k*-NN can guarantee model accuracy more than 90% while the prediction accuracies of the models based on CART are 82.05% for the front top excitation and 86.15% back bottom excitation, respectively. The main reason contributing to this phenomenon is that the decision made by CART is mainly on basis of the expectation, and unreasonable expectation is able to result in errors and inaccurate diagnosis of developed tree model. In addition, the *k*-NN has the best perdition accuracy due to its outstanding capacity of

nonlinear classification, which is still robust to noisy training data. For the diagnosis results, it is noticeable that models trained by the GW data measured from back excitations have better diagnosis performance than the models developed based on the data from top excitation cases. The potential reason for this outcome is that the front top excitation location is close to the top accelerometer (S1), so the top sensors may collect more surface waves (vibration) than flexural waves, which can affect the diagnosis performance of the model. Among all the models, the optimal one is the *k*-NN model trained by the data from back top excitation, with the diagnosis accuracy of 97.95%, which has been highlighted in bold in Table 2. In summary, the models developed by three machine learning algorithms are capable of providing satisfactory diagnosis results, which accords with the diagnosis requirement of pole assess management industry.

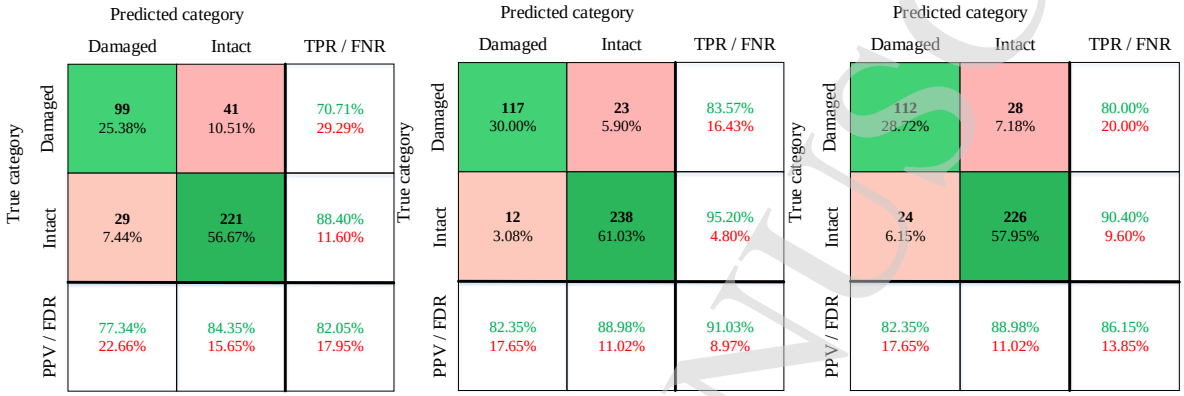

(a) (b) (c)

Fig. 17.Confusion matrix ofCART model for health condition diagnosis of wood poles: (a) front top excitation, (b) back top excitation and (c) back bottom excitation.

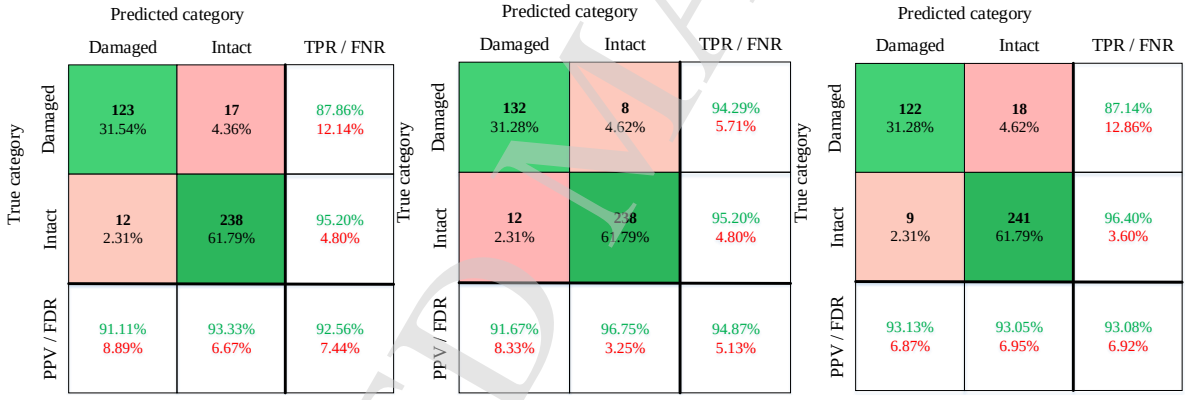

(a) (b) (c)

Fig. 18.Confusion matrix of SVM model for health condition diagnosis of wood poles: (a) front top excitation, (b) back top excitation and (c) back bottom excitation.

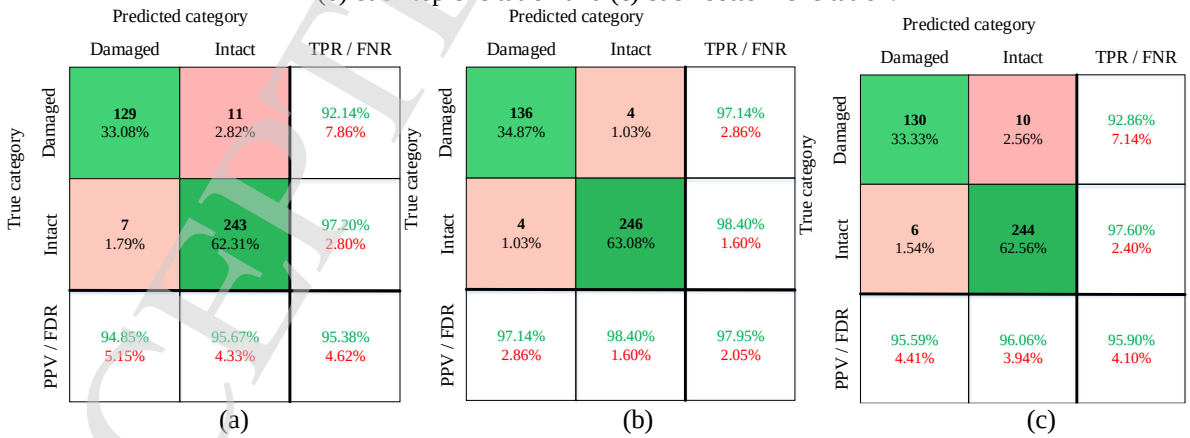

(a) (b) (c)

Fig. 19.Confusion matrix of *k*-NN model for health condition diagnosis of wood poles: (a) front top excitation, (b) back top excitation and (c) back bottom excitation.

Table 2 Diagnosis accuracy of different machine learning models

Method	Excitation location		
	Front top	Back top	Back bottom
CART	82.05%	91.03%	86.15%
SVM	92.56%	94.87%	93.08%
k-NN	95.38%	**97.95%**	95.90%

5. Conclusions

This paper presenteda novel intelligent NDE framework for in-situ health diagnosis of wood electricity poles, consisting of multi-sensing, advanced signal processing and state-of-the-art ML techniques. In the proposed framework, the MEMD method is proposed to accurately decompose the transverse wave signals, which can prevent the mode mixing problem in standard EMD. To evaluate the superiority of the developed MEMD over standard EMD, a comparative study is conducted on the simulated signals. The comparison results show that the presented MEMD outperforms the EMD in extracting effective IMFs and eliminating pseudo IMFs, even when the processed signals are polluted with high SNR white Gaussian noises. Then, the feature information of the IMFs is extracted as the signal features that are sensitive to the damage, and the PCA is adopted to choose the best features as inputs to develop the diagnosis models, which are based on CART, SVM and *k*-NN. To appraise the capacity of the proposed framework,15 new poles and 24decommissioned poles with different condition scenarioswere tested in the field, and the GW datacollected by a portable multi-sensing system were used for performance evaluation. The results show that as the main features, the selected first 10 PCs are effective in identifying different health conditions of tested pole. Besides, among three types of machine learning models, the *k*-NN performs the best, with the diagnosis accuracy as high as 97.95%. On the whole,the performance of the proposed intelligent framework for the pole condition diagnosis is promising, which meets the asset management requirement of pole industry.

Acknowledgements

This research is supported by Australian Research Council via Linkage Project (LP110200162)) and Industrial Transforming Research Hub for Nanoscience Based Construction Materials Manufacturing (IH150100006) as well as Ausgrid. The authors greatly appreciate the financial and technical supports from the funding bodies.

References

1. S.Bandara, P. Rajeev, E.Gad, B.Sriskantharajah and I.Flatley, Damage detection of in service timber poles using Hilbert-Huang transform, *NDT&E Int.***107** (2019) 102141.
2. M. Nguyen, G. Foliente and X. Wang, State-of-the-practice and challenges in non-destructive evaluation of utility poles in service, *Key Eng. Mater.***270–273** (2004) 1521–1528.
3. L. Francis and J. Norton, *Australian timber pole resources for energy networks. A review*, Technical Report, Department of Primary Industries and Fisheries, Queensland, (2006).
4. S.Mudiyanselage, P. Rajeev, E.Gad, B.Sriskantharajah and I.Flatley, Application of stress wave propagation technique for condition assessment of timber poles, *Struct. Infrastruct. E.***15** (9) (2019) 1234–1246.
5. Y. Yu and N. Yan, Numerical study on guided wave propagation in wood utility poles: Finite element modelling and parametric sensitivity analysis, *Appl. Sci.***7** (10) (2017) 1063.
6. J.Li, M.Subhani and B.Samali, Determination of embedment depth of timber poles and piles using wavelet transform, *Adv. Struct. Eng.***15** (5) (2012) 759–770.
7. T.Nguyen, T.H.T.Chan, D.P. Thambiratnam and L.King, Development of a cost-effective and flexible vibration DAQ system for long-term continuous structural health monitoring, *Mech. Syst. Signal Pr.***64–65** (2015) 313–324.
8. A. Nguyen, K.A.T.L.Kodikara,T.H.T. Chan and D.P.Thambiratnam, Deterioration assessment of buildings using an improved hybrid model updating approach and long-term health monitoring data, *Struct. Health Monit.***18** (1) (2019) 5–19.
9. K.-F. Lo, S.-H. Ni and Y.-H. Huang, Non-destructive test for pile beneath bridge in the time, frequency, and time-frequency domains using transient loading, *Nonlinear Dynam.***62** (1–2) (2010) 349–360.
10. J.F. Doyle, *Wave Propagation in Structures*/ (Springer, New York, 1989).
11. M.Subhani, J. Li and B.Samali, A comparative study of guided wave propagation in timber poles with isotropic and transversely isotropic material models, *J. Civ. Struct. Health Monit.***3** (2) (2013) 65–79.
12. M.Legg and S.Bradley, Measurement of stiffness of standing trees and felled logs using acoustics: A review, *J. Acoust. Soc. Am.***139** (2) (2016) 588–604.

13. Y.Yang, C.-T.Ng and A.Kotousov, Second harmonic generation of guided wave at crack-induced debonding in FRP-strengthened metallic plates, *Int. J. Struct. Stab. Dyn.***19** (1) (2019) 1940006.
14. R.Guan, Y.Lu, K. Wang and Z.Su, Fatigue crack detection in pipes with multiple mode nonlinear guided waves, *Struct. Health Monit.***18** (1) (2019) 180–192.
15. R.C.Sriramadasu, Y.Lu and S.Banerjee, Identification of incipient pitting corrosion in reinforced concrete structures using guided waves and piezoelectric wafer transducers, *Struct. Health Monit.***18** (1) (2019) 164–171.
16. Y.Yang, C.-T.Ng and A.Kotousov,Bolted joint integrity monitoring with second harmonic generated by guided waves, *Struct. Health Monit.***18** (1) (2019) 193–204.
17. H.Kolsky, Stress waves in solids, *J. Sound Vib.***1** (1) (1964) 88–100.
18. H. Wang, Theoretical evaluation of embedded plate-like and solid cylindrical concrete structures with guided waves, PhD thesis, Northwestern University, USA (2004).
19. D. Royer and E. Dieulesaint,*Elastic Waves in Solids I: Free and Guided Propagation*/ (Springer, New York, 1989).
20. K.F. Graff, *Wave Motion in Elastic Solids*/ (Dover Publications, United States, 2012).
21. J. James J. Lynch, Experimental verification of flexural guided waves in concrete cylindrical piles, PhD thesis, Northwestern University, USA (2007).
22. M. Subhani, J.C. Li, H. Gravenkamp and B. Samali, Effect of elastic modulus and poisson's ratio on guided wave dispersion using transversely isotropic material modelling, *Adv. Mater. Res.***778** (2013) 303–311.
23. N.E. Huang, Z. Shen, S.R. Long, M.C. Wu, H.H. Snin, Q. Zheng, N.C. Yen, C.C. Tung and H.H. Liu, The empirical mode decomposition and the Hilbert spectrum for nonlinear and non-stationary time series analysis, *Proc. R. Soc. London Ser. A- Math. Phy. Eng. Sci.***454** (1971) 903–995.
24. Y.Xin, H.Hao and J.Li, Time-varying system identification by enhanced Empirical Wavelet Transform based on Synchroextracting Transform, *Eng. Struct.***196** (2019) 1093313.
25. Y.Xin, H.Hao and J.Li, Operational modal identification of structures based on improved empirical wavelet transform, *Struct. Control Hlth.***26** (3) (2019) e2323.
26. J. Li and H. Hao, Damage detection of shear connectors under moving loads with relative displacement measurements, *Mech. Syst. Sig. Process.***60** (2015) 124–150.
27. J. Li and H. Hao, Health monitoring of joint conditions in steel truss bridges with relative displacement sensors, *Measurement* **88** (2016) 360–371.
28. H.-W.Ma, Y.-Z.Lin and Z.-H.Nie, Physical interpretation of principal component analysis for structural dynamics through string vibration, *Int. J. Struct. Stab. Dyn.***19** (9) (2019) 1950109.
29. S.Ma, J.Li, H.Hao and S.Jiang, Structural response recovery based on improved multi-scale principal component analysis considering sensor performance degradation, *Adv. Struct. Eng.***21** (2) (2018) 241-255.
30. R.Chester, M.Khondoker, L.Shepstone, J.S.Lewis and C.Jerosch-Herold, Self-efficacy and risk of persistent shoulder pain: Results of a Classification and Regression Tree (CART) analysis, *Brit. J. Sport Med.***53** (13) (2019) 825–834.
31. S.R.F.de Mello, C.Manapragada and A.Bifet, Measuring the Shattering coefficient of Decision Tree models, *Expert Syst. Appl.***137** (2019) 443–452.
32. H.W.J.Reeve and A.Kabán, Robust randomized optimization with k nearest neighbors, *Anal. Appl.***17** (5) (17) 819–836.
33. Etedali and N.Mollayi, Cuckoo search-based least squares support vector machine models for optimum tuning of tuned mass dampers, *Int. J. Struct. Stab. Dyn.***18** (2) (2018) 1940006.
34. Y. Yu, W. Li, J. Li and T.N. Nguyen, A novel optimised self-learning method for compressive strength prediction of high performance concrete, *Constr. Build. Mater.***184** (2018) 229–247.